European Journal of Pharmacology 634 (2010) 16–25

Contents lists available at ScienceDirect

European Journal of Pharmacology

journal homepage: www.elsevier.com/locate/ejphar

Molecular and Cellular Pharmacology

Galantamine inhibits slowly inactivating K^+ currents with a dual dose–response relationship in differentiated N1E-115 cells and in CA1 neurones

M. Inês Vicente [1], Pedro F. Costa, Pedro A. Lima *

Faculdade de Ciências Médicas, Universidade Nova de Lisboa, Campo Mártires da Pátria, 130, 1169-056 Lisboa, Portugal

ARTICLE INFO

Article history:
Received 16 June 2009
Received in revised form 26 January 2010
Accepted 13 February 2010
Available online 23 February 2010

Keywords:
Galantamine
Acetylcholinesterase inhibitor
Alzheimer's disease
Hippocampus
Neuroblastoma
Voltage-clamp artefact

ABSTRACT

Galantamine, one of the major drugs used in Alzheimer's disease therapy, is a relatively weak acetylcholinesterase inhibitor and an allosteric potentiating ligand of nicotinic acetylcholine receptors. However, a role in the control of excitability has also been attributed to galantamine via modulation of K^+ currents in central neurones. To further investigate the effect of galantamine on voltage-activated K^+ currents, we performed whole-cell voltage-clamp recordings in differentiated neuroblastoma N1E-115 cells and in dissociated rat CA1 neurones. In both cell models, one can identify two main voltage-activated K^+ current components: a relatively fast inactivating component (*I*fast; time constant ≈ hundred milliseconds) and a slowly inactivating one (*I*slow; time constant ≈ 1 s). We show that galantamine (1 pM–300 μM) inhibits selectively *I*slow, exhibiting a dual dose–response relationship, in both differentiated N1E-115 cells and CA1 neurones. We also demonstrate that, in contrast with what was previously reported, galantamine-induced inhibition is not due to a shift on the steady-state inactivation and activation curves. Additionally, we characterized a methodological artefact that affects voltage-dependence as a function of time in whole-cell configuration, observed in both cell models. By resolving an inhibitory role on K^+ currents in a non-central neuronal system and in hippocampal neurones, we are attributing a widespread role of galantamine on the modulation of cell excitability. The present results are relevant in the clinical context, since the effects at low dosages suggest that galantamine-induced K^+ current inhibition may contribute to the efficiency of galantamine in the treatment of Alzheimer's disease.

1. Introduction

It has long been demonstrated that the degeneration of cholinergic neurones in the basal forebrain may be partially responsible for the learning and cognitive deficits observed in patients with Alzheimer's disease (Bartus et al., 1982; Francis et al., 1999). The recognition of cholinergic dysfunction in Alzheimer's disease led to the development of drugs that enhance cholinergic function, mainly by inhibition of the catabolic enzyme, acetylcholinesterase (AChE). One such compound is galantamine, a selective competitive, reversible and relatively weak AChE inhibitor (Lilienfeld, 2002; Thomsen et al., 1991; Thomsen and Kewitz, 1990), that has also been described as an allosteric potentiating ligand of nicotinic receptors (Schrattenholz et al., 1996; Maelicke et al., 1997; Samochocki et al., 2000). As a result of the allosteric potentiation of nicotinic acetylcholine receptors, galantamine has been shown to enhance GABA and glutamate release in hippocampal slices (Santos et al., 2002). Additionally, galantamine has been proven to potentiate the NMDA receptor whole-cell current in cortical neurones (Moriguchi et al., 2004), to stimulate dopamine release in striatal slices (Zhang et al., 2004b) and to enhance dopaminergic (Schilstrom et al., 2007) and purinergic neurotransmission (Caricati-Neto et al., 2004).

An alternative hypothesis to explain synaptic facilitation by galantamine has been linked to galantamine-induced changes in neuronal excitability. There is evidence that galantamine can increase excitability by inhibiting postburst afterhyperpolarization (AHP) and accommodation of CA1 hippocampal pyramidal neurones, via modulation of muscarinic transmission (Oh et al., 2006). Moreover, galantamine reduces delayed rectifier K^+ current ($I_{K(DR)}$) in acutely dissociated rat hippocampal pyramidal neurones (1–100 μM galantamine; (Pan et al., 2003b) and in cloned Kv2.1 channel current (0.1–100 μM; (Zhang et al., 2004a). In both studies, hyperpolarizing shifts on the activation and steady-state inactivation curves were reported under 10 μM galantamine; such shifts are not coherent with galantamine-induced current reduction. The inhibition of central outward K^+ currents by other AChE inhibitors currently used in Alzheimer's disease therapy—tacrine (Li and Hu, 2002), rivastigmine (Pan et al., 2003a) and donepezil (Yu and Hu, 2005)—has also been reported. Altogether, these data suggest that the reduction of K^+

* Corresponding author. Present address: Centro de Quimica e Bioquimica, Faculdade de Ciências, Universidade de Lisboa, Campo Grande, 1749-016 Lisboa, Portugal. Tel.: +351 963807571; fax: +351 21 7500088.
E-mail address: palima@fc.ul.pt (P.A. Lima).
[1] Present address: Champalimaud Neuroscience Programme, Instituto Gulbenkian de Ciência, Rua da Quinta Grande 6, 2780-156 Oeiras, Portugal.

0014-2999/$ – see front matter © 2010 Elsevier B.V. All rights reserved.
doi:10.1016/j.ejphar.2010.02.021

currents in the brain may provide a mean of enhancing cognitive function in Alzheimer's disease. In fact, it was demonstrated that by modulating some K^+ channels, one can tune long term potentiation (LTP; Ramakers and Storm, 2002; Chen et al., 2006)—the experimental paradigm of memory (reviewed in Lisman, 2003), or improve cognitive deficits when memory is impaired (Inan et al., 2000). Indeed, treatment of aged rats with galantamine has been shown to extend LTP decay (Barnes et al., 2000).

It has been reported that mean galantamine plasma concentrations of Alzheimer's disease patients, when sampled within 10 h of administration, ranged from 82 μg/l to 126 μg/l (223–342 nM) (Raskind et al., 2000; Wilcock et al., 2000; Farlow, 2003). However, according to the studies described before concerning galantamine effects on K^+ conductances (Oh et al., 2006; Pan et al., 2003b; Zhang et al., 2004a), with such range of concentrations (223–342 nM), only marginal effects were observed.

Therefore, in the present report we aimed to study the effect of galantamine on voltage-activated K^+ currents, using a wider range of concentrations, with doses of galantamine ranging from subnanomolar to micromolar. Two different cell models were used: differentiated neuroblastoma N1E-115 cells—a cell line from the sympathetic nervous system—and acutely dissociated rat hippocampal pyramidal neurones from the CA1 region. It is presently shown that galantamine (1 pM–300 μM) selectively inhibits a slowly inactivating K^+ current in both cell models, exhibiting dual dose–response relationships. We also show that this current inhibition is not due to a shift in the voltage-dependence of steady-state inactivation and activation. The present work extends our understanding about how galantamine acts at the nerve cell.

2. Materials and methods

2.1. Neuroblastoma cell-culture and isolation of CA1 neurones

Mouse neuroblastoma cells of the clone N1E-115 (ECACC, 88112303) were routinely grown in Dulbbecco's modified Eagle medium (DMEM) supplemented with 10% fetal bovine serum (FBS) and 0.1% antibiotic (10 000 U/ml penicillin and 10 000 μg/ml streptomycin). The cultures were maintained at 37 °C in a humidified atmosphere containing 5%CO_2. Cells were split weekly when 70–80% confluent and were plated in 35 mm plastic Petri dishes (Nunc) using medium containing reduced serum content—2.5% FBS—and 1.5% dimethyl sulphoxide (DMSO), for induction of neuronal differentiation. Cells at 6–14 days after induction of differentiation, showing clear neuritic processes, were selected for recording.

Hippocampal pyramidal cells from the mid-third CA1 region of P21-30 Wistar rats were isolated as described before (Costa et al., 1994). Sub-slices of the CA1 region were incubated at 32 °C in an oxygen saturated solution under moderate stirring; the composition of the incubating solution was as follows (in mM): NaCl 120, KCl 5, CaCl2 1, MgCl2 1, 1,4-Piperazinediethanesulfonic acid (PIPES) 20, D-Glucose 25, adjusted to pH 7 with 1 mM NaOH. Trypsin (0.6 mg/ml) was added to this solution shortly after the preparation of the sub-slices; incubation period was 30–50 min, depending on rat's age. Sub-slices were transferred to an oxygen saturated enzyme-free solution after a brief wash with this solution and kept at room temperature at moderate stirring. A trypsin inhibitor (0.5 mg/ml) was added to the enzyme-free solution; the preparation remained viable for about 5–6 h. Cells from the CA1 layer were isolated by gentle trituration of the sub-slices using fire polished Pasteur pipettes (1.5–2 mm bore).

2.2. Electrophysiological recordings

The 35 mm plastic Petri dishes were used as recording chambers for either cultured or acutely isolated cells. Voltage-clamp recordings were performed in the whole-cell patch clamp configuration. Patch pipettes (1.5–3 MΩ), pulled from borosilicate glass (Science Products GmbH, GB150T-8P), were filled with pipette solution (N1E-115-cells) containing (in mM): $KMeSO_4$ 140, $Na_{1/2}$HEPES 10, $CaCl_2$ 1, $MgCl_2$ 1, EGTA 10, Na_2ATP 2, NaGTP 0.4 and adjusted to pH 7.2–7.3 with 1 mM NaOH (calculated free $[Ca^{2+}] = 60$ nM, by Webmaxclite 1.15, MaxChelator). In the case of recordings in CA1 neurones, modifications of the above solution were used, as follows: $KMeSO_4$ was either 132 mM or replaced by KF 140 mM (osmolarity was kept within the same range).

The recording chamber was perfused by gravity (2–3 ml/min) with the following solution (in mM): NaCl 135, KCl 5.4, $Na_{1/2}$HEPES 10, $CaCl_2$ 2, $MgCl_2$ 1.5, D-Glucose 25 and adjusted to pH 7.4 with 1 mM KOH (calculated equilibrium potential for K^+ was −82 mV). Tetrodotoxin (TTX) (50 nM) was added to the external solution in most of the experiments. During recording, cells were kept near the surface and remained under continuous bath perfusion. The estimated junction potential for the filling and bath solution combinations mentioned above is, respectively, −9.8 mV, −9.4 and −9.2 mV (calculated with JPCalc 2.00, School of Physiology and Pharmacology University of New South Wales). Data were not corrected for the junction potential.

Currents were recorded with an Axopatch 200B electrometer (Axon Instruments) and stored using a DigiData 1200 interface (Axon Instruments) and pCLAMP 6.0.3 software (Axon Instruments) Signals were filtered at 2 kHz (−3 dB, four pole Bessel) with a 5 kHz sampling rate. Series resistance was compensated to about 70%. Electrode and cell membrane capacitances were compensated. Leak subtraction was applied to raw data during data processing (see below). Experiments were carried out at room temperature (about 20 °C).

2.3. Experimental design (voltage protocols)

In experiments with N1E-115 cells, current amplitude and clamp conditions were monitored throughout the experiment with a set of two 5.6 s in duration depolarizing pulses to 0 mV and +40 mV, every 60 s. For the study of the voltage-dependence of activation a set of 6.4 s command pulses from −60 mV to +50 mV (in 10 mV steps) was applied. For the subsequent estimate of leak current, a set of pulses (−75 mV to −53 mV, 2 mV increments, 100 ms) was applied prior (60 ms) to the command pulses. This allowed calculating and subtracting leak current at each voltage. For the study of steady-state inactivation, currents were evoked by a 4.8 s in duration depolarizing command pulse to a fixed voltage (+40 mV) preceded by 6.4 s prepulses ranging from −60 mV to +50 mV (in 10 mV steps). The holding potential was −70 mV.

In experiments with CA1 neurones, the voltage-clamp protocols were equivalent to those described above, differing as follows. A hyperpolarizing pre-pulse to −120 mV, 200 ms in duration, was used. Such pre-pulse aimed the removal of inactivation of channels underlying the fast current component (previously named A–D type). Current amplitude and clamp conditions were monitored throughout the experiment with a set of two 2.1 s in duration depolarizing pulses to −30 mV and +40 mV, every 60 s. To study the fast current component in isolation, a different voltage protocol was used: the same depolarizing pulse to +40 mV (2 s, holding potential −50 mV) was preceded either by a pre-pulse to −30 mV or −120 mV, with a duration (30–200 ms) that was adjusted to each cell/current; the subsequent current traces were subsequently subtracted and, thus, the fast current was then isolated (Lima et al., 2008; see inset in Fig. 2B).

For the study of the voltage-dependence of activation a set of 1 s command pulses from −70 mV to +50 mV (in 10 mV steps) was applied; command pulses were preceded by a set of 160 ms prepulses from −70 mV to −52 mV (2 mV increments), to subsequently estimate and subtract leak current. For the study of steady-state inactivation, currents were evoked by a 4 s in duration depolarizing command pulse to a fixed voltage (+40 mV) preceded by 640 ms

prepulses ranging from −140 to +10 mV (in 10 mV steps). The holding potential was −60 mV.

2.4. Data analysis and statistical procedures

Data were analyzed using pCLAMP Clampfit 9.0.1.07 (Axon Instruments), Microcal^{MT} Origin^{MT} 5.0 (Microcal Software) and GraphPad Prism 4.00 (GraphPad Software) software.

For each experiment, the decaying phase of the K^+ current was best fitted with a sum of two exponential functions, using the following equation:

$$F(t) = A_{fast} \exp(-t/\tau_{fast}) + A_{slow} \exp(-t/\tau_{slow}) + c, \quad (1)$$

where τ_{fast} and τ_{slow} are the time constants of the fast and the slow-inactivating current components, respectively; A_{fast} and A_{slow} are coefficients and C is a constant.

Currents were measured as shown in Figs. 1Ai and 2Ai. Current amplitude at the peak was used as a measure of the fast component; the measure of the slow component was taken as the current amplitude at a time equal to $5\tau_{fast}$ after the start of the command pulse.

In the case of activation, the current amplitudes of the fast and slow components were converted to conductance (G) using the equation:

$$G = I/(V-E_K), \quad (2)$$

where I is the current amplitude, V is the step command potential and E_K is the estimated equilibrium potential for K^+. Conductance values were normalized for the maximal response (G/Gmax) and plotted against step command potential (V); normalized data points were fitted with the following equation:

$$G/G\,\mathrm{max} = (A_1-A_2)/\left\{1 + \exp\left[\left(V-V_{1/2}\right)/V_s\right]\right\} + A_2, \quad (3)$$

where $V_{1/2}$ is the half-activation potential, V_s is the slope constant, A_1 and A_2 are coefficients.

For inactivation, current values were normalized to maximal value (I/Imax) and plotted against pre-pulse potential (V). Normalized data points were fitted with the following Boltzmann equation:

$$I/I\,\mathrm{max} = (A_1-A_2)/\left\{1 + \exp\left[\left(V-V_{1/2}\right)/V_s\right]\right\} + A_2. \quad (4)$$

For the comparison of data before and under galantamine, the Wilcoxon signed-rank test ($n<10$) or the paired t-test ($n\geq 10$) was used. Student t-test was applied for the comparison between results of the application of galantamine at different concentrations. Differences were considered significant if $P<0.05$. Values given in the text are mean ± S.E.M.

For the quantification of current inhibitions induced by galantamine, the following analysis was conducted: the current trace recorded under treatment with galantamine (after effect stabilised) was subtracted from control trace (before addition); the charge of the consequent galantamine-sensitive current was calculated (integral) and compared with the charge of the control current; effect is presented as % current inhibition.

2.5. Drugs and chemical reagents

Reagents were obtained from Merck, unless specified: DMEM, FBS, penicillin, streptomycin and trypsin-EDTA were purchased from Gibco; DMSO, $Na_{1/2}$HEPES, EGTA, Na_2ATP, NaGTP, PIPES, trypsin type XI, trypsin inhibitor and galantamine (G1660) from Sigma; TTX from Alomone Labs; and $KMeSO_4$ from AcrösOganics.

Galantamine was used in concentrations of 1 pM to 300 μM. Concentrated stock solutions of galantamine (100 nm, 100 μM and 10 mM) were prepared in water and stored at −20 °C and subsequently diluted in the superfusing bath solution to the required final concentration.

3. Results

3.1. K^+ currents in differentiated N1E-115 cells and in dissociated CA1 neurones

Fig. 1Ai and Bi depict currents evoked by a depolarising command pulse to +40 mV in differentiated N1E-115 cells and in dissociated CA1 neurones. In either case this evoked a fast rising outward K^+ current with a slow decay. In both cell models, and given the long duration of the command pulse, the decaying phase of the K^+ current was best described by a sum of two exponential functions (Eq. (1)), indicating the existence of at least two current components: a relatively fast inactivating current, here termed *I*fast, and a slowly inactivating one, *I*slow (these current components were characterized by us before: Lima et al. (2008) for differentiated N1E-115 cells; Costa et al. (1994) for CA1 neurones. In the cases illustrated in Fig. 1Ai and Bi, the inactivation time constants of the two current components were: $\tau_{fast}=64$ ms, $\tau_{slow}=1741$ ms, for the N1E-115 cell (Fig. 1Ai); $\tau_{fast}=70$ ms, $\tau_{slow}=1015$ ms, for the CA1 neurone (Fig. 1Bi). Fig. 1Aii–iii and Bii–iii depict K^+ currents evoked by the protocols (insets) used to characterize the voltage-dependence of activation and steady-state inactivation in differentiated N1E-115 cells and in CA1 neurones, respectively.

3.2. Effect of galantamine on the slow component in differentiated N1E-115 cells and in dissociated CA1 neurones

To observe the effect of galantamine on current amplitude, currents were evoked throughout the experiment with a depolarizing pulse to +40 mV (voltage protocols as in Figs. 1Ai and 1Bi). Fig. 2Bi and Aii show the effect of galantamine in differentiated N1E-115 cells, before and under 100 pM and 10 μM, respectively; the choice of these two concentrations relates to the dose–response relationship found for galantamine (see below, Fig. 2C). The effect of galantamine could be detected 3–4 min after drug application and reached a steady-state in 10–15 min (not shown).

From the current traces in Fig. 2Ai and Aii it is apparent that galantamine had a selective effect on *I*slow, leaving *I*fast unaffected. Analysis of the effect of galantamine on the inactivation kinetics of the two current components, revealed that the time constants values of *I*fast did not change under application of 100 pM or 10 μM, further demonstrating that galantamine has a selective effect on *I*slow. Mean values concerning experiments as illustrated in Fig. 2Ai and Aii were as follows: in control: τ(fast) = 91.8 ± 10.8, τ(slow) = 1861.5 ± 199.8; under 100 pM galantamine: 99.3 ± 11.0 ms and 1398.4 ± 139.4 ms, respectively ($n=13$); in control: τ(fast) = 57.8 ± 4.0 ms, τ(slow) = 1745.7 ± 132.0; under 10 μM galantamine: 61.3 ± 4.7 ms and 1373.5 ± 108.1 ms, respectively ($n=13$). Under 100 pM and 10 μM, τ(slow) values, but not τ(fast) values, differed statistically from the corresponding control values (paired t-test). Current subtractions, as illustrated in Fig. 2Ai and Aii (A–B), revealed a slow-rising and slow-inactivating galantamine-sensitive current. The inactivation of the galantamine-sensitive component, for both concentrations, was best described by a single exponential (Eq. (1), with only one term), with time constants of the same order of magnitude as the time constant of *I*slow; mean time constants were as follows: 2479 ± 161.0 ms (n = 11) and 2319 ± 158.3 ms (n = 10), for 100 pM and 10 μM galantamine, respectively. Mean values concerning the application of 100 pM and 10 μM galantamine did not differ statistically (Student t-test). This strongly suggests that the nature of current sensitive to galantamine is the same when 100 pM or 10 μM galantamine is used.

The dose–response relationship for the inhibitory effect of galantamine on *I*slow in differentiated N1E-115 cells is depicted in

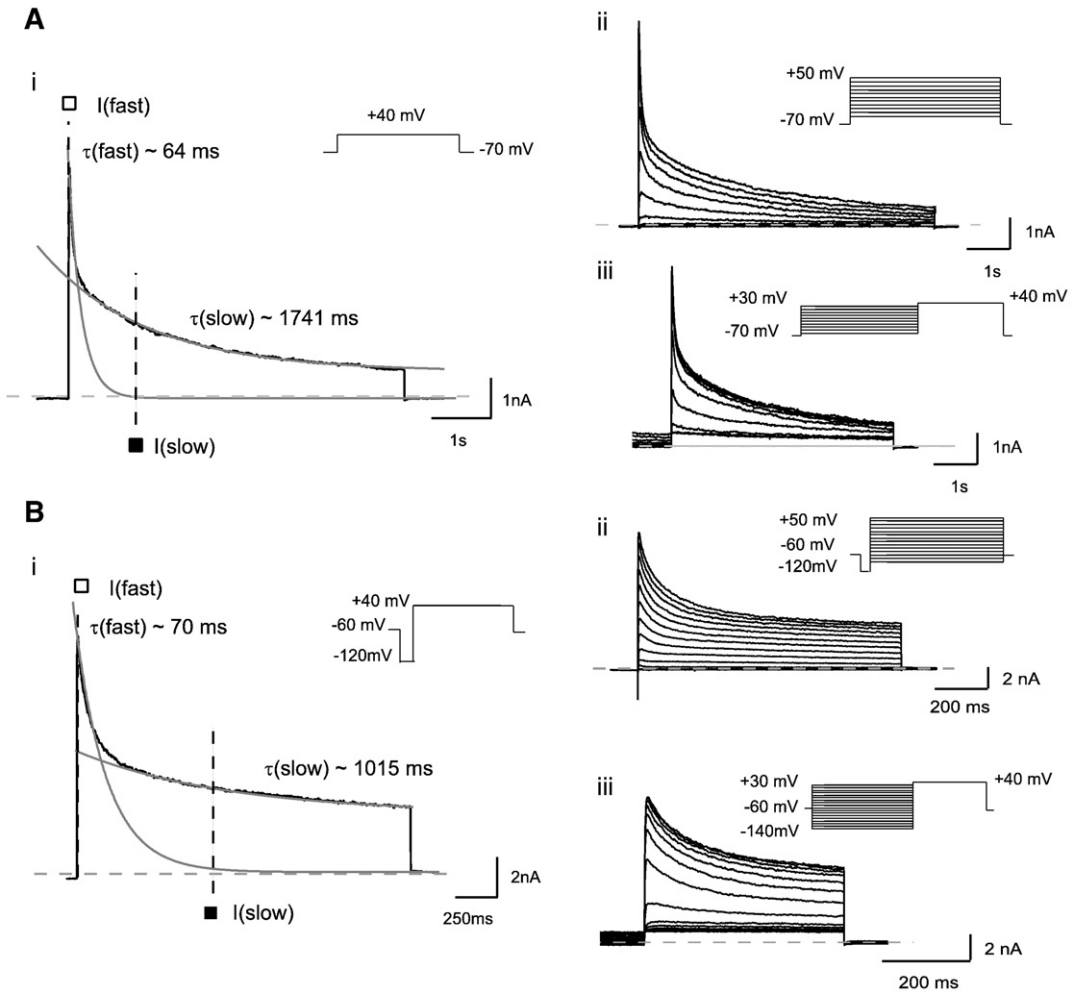

Fig. 1. Voltage-activated K^+ current components evoked in differentiated neuroblastoma N1E-115 cells (A) and in dissociated CA1 pyramidal neurones (B). (Ai) Total outward K^+ current in a differentiated N1E-115 cell evoked by a depolarizing pulse to +40 mV (5.6 s in duration) from holding potential of −70 mV (inset). The decaying phase of the K^+ current is best described by a sum of two exponential functions (Eq. (1)). Peak current amplitude (□) was used as a measure of the fast component; the amplitude of the slow component was taken at a time equal to $5^*\tau_{fast}$ after the start of the command pulse (■). (Aii) K^+ currents evoked by a set of depolarizing command pulses (6.4 s) in steps of 10 mV (range −50 mV to +50 mV), from a holding potential of −70 mV (inset). (Aiii) K^+ currents evoked by a command step to +40 mV (4.8 s) following a set of prepulses (6.4 s) ranging from −60 mV to +30 mV in steps of 10 mV, for the study of steady-state inactivation; holding potential of −70 mV (inset). (B) K^+ currents evoked in a dissociated CA1 pyramidal neurone. Voltage-clamp protocols were equivalent to those described in (a), with a hyperpolarizing pre-pulse to −120 mV, 200 ms in duration (Bi, Bii); holding potential was −60 mV in all cases. The procedures for the measurements of current amplitude (Bi) were the same as in (Ai). (Biii) The voltage-clamp protocol applied for the study of steady-state inactivation had prepulses ranging from −140 mV to +30 mV (steps in 10 mV).

the plot of Fig. 2C (square symbols); the results concern experiments with doses of galantamine ranging from 1 pM to 300 μM. The effect, which was concentration-dependent, exhibits a dual relationship (Fig. 2C). It is important to note that even at the concentrations that induce the highest inhibitions, the effect was not complete (23.3 ± 5.2% at 100 pM; 36.4 ± 8.5% at 300 μM).

The effect of galantamine in CA1 neurones was tested at three key-concentrations: 100 pM, 10 μM (representative of both phases of the dose–response relationship in N1E-115 cells) and 100 nM (corresponding to the minimal effect). Fig. 2Bi and Bii illustrate the result of the application of 100 pM and 10 μM, respectively, in two CA1 neurones. It is noticeable that in CA1 neurones the effect of galantamine is of the same nature we found for the N1E-115 cells, i.e. only the slow component was affected. To confirm the specificity of the galantamine effect on *I*slow in CA1 pyramidal neurons, we applied voltage protocols that aim to dissect the two current components (see Materials and methods). In isolation, *I*fast was not altered by 10 μM galantamine ($n = 3$) (Fig. 2B, inset). Most importantly, the galantamine-induced current reduction showed a similar trend in terms of dose–response relationship to the one observed in differentiated N1E-115 cells (Fig. 2C; triangle symbols).

For the experiments in CA1 pyramidal neurones a fluoride-based internal solution was used (see Materials and methods); this provided better current stability in these cells, which was critical for long lasting recordings during drug application. Given the eventual influence of fluoride on some cellular mechanisms—such as G-protein mediated signalling (Pleumsamran et al., 1998)—these experiments were carried out also with a different pipette solution: a $KMeSO_4$-based filling solution (see Materials and methods) for comparison. The same inhibitory effect of galantamine on *I*slow was observed with either filling solutions, with similar percent reductions and dose–relationship patterns (Fig. 2C); the absence of effect on *I*fast was not dependent on the chloride substitute of the filling solution.

For any of the concentrations of galantamine used, none of the effects recovered upon wash.

3.3. Artefacts in the steady-state inactivation and activation—criteria for drug application

In the course of the study of the effect of galantamine on the voltage-dependence of steady-state inactivation and activation, we were

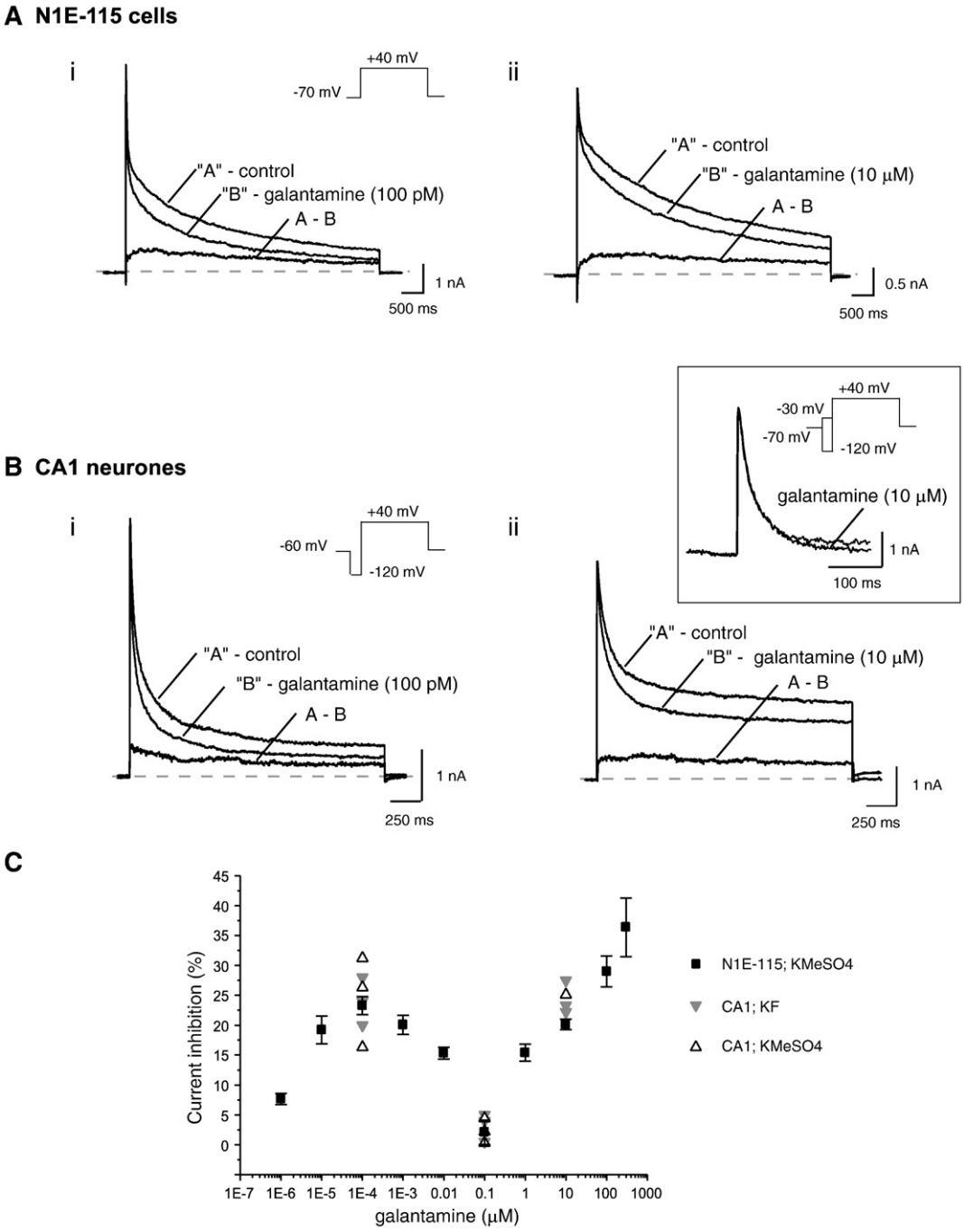

Fig. 2. Specific effect of galantamine on the slow component in differentiated N1E-115 cells (A) and in CA1 pyramidal neurones (B). (Ai, Aii) Current traces evoked by a depolarizing command pulse to +40 mV (voltage protocol as in Fig. 1Ai) before and under application of 100 pM and 10 μM galantamine, respectively, in two differentiated N1E-115 cells. (Ai) inactivation time constants in control were as follows: τ(fast) = 91.4 ms, τ(slow) = 1893.3 ms; under 100 pM galantamine: 103.1 ms, 1867.2 ms, respectively; the time constant of the galantamine-sensitive component (A–B) was 2271 ms (Aii) in control: τ(fast) = 125.8 ms, τ(slow) = 1143.5 ms; under 10 μM galantamine: 133.7 ms, 1243.9 ms, respectively; the time constant of the galantamine-sensitive component (A–B) was 2282 ms (Bi, Bii) effect of 100 pM and 10 μM galantamine, respectively, in two CA1 neurones (voltage protocol as in Fig. 1Bi). (Bi) inactivation time constants in control were as follows: τ(fast) = 41.9 ms, τ(slow) = 405.2 ms; under 100 pM galantamine: 43.8 ms, 379.2 ms, respectively; the time constant of the galantamine-sensitive component (A–B) was 473 ms. (Bii) in control: τ(fast) = 71.5 ms, τ(slow) = 476.2 ms; under 10 μM galantamine: 68.4 ms ms, 427.9 ms, respectively; the time constant of the galantamine-sensitive component (A–B) was 1751.3 ms. Inset: galantamine did not alter *I*fast in isolation. Currents evoked by a depolarizing step to +40 mV (holding potential −50 mV) which was preceded either by a pre-pulse to −30 mV or −120 mV; this voltage protocol was applied before and under 10 μM galantamine. The subsequent current subtraction (shown in the inset) aimed the isolation of the fast current component. (C) Effect of galantamine on the slow component in differentiated N1E-115 cells expressed as a dose–response relationship (filled squares); values are expressed as mean ± S.E.M.; sample size concerning N1E-115 experiments were as follows: 1 pM, n = 4, 10 pM, n = 5; 100 pM, n = 14; 1 nM, n = 3; 10 nM, n = 3; 100 nM, n = 4; 1 μM, n = 5; 10 μM, n = 15; 100 μM, n = 3.; sample size concerning CA1 experiments conducted with the two pipette solutions can be depicted from figure (open triangles—KMeSO4 based pipette solution, n = 3 for the three key-concentrations; filled triangle—KF based pipette solution, n = 3 for the three key-concentrations). All experiments concern sole treatments for each cell (galantamine was not applied in increasing concentrations). All experiments started after 30–45 min recording to account for the voltage shifts described (Fig. 3, Table 1); galantamine application was just applied after a negligible current run-up being observed (described in Fig. 3Ai and Bi).

confronted with an important experimental artefact, independent of drug effect, which affected voltage profiles as a function of time after whole-cell configuration, and thus we herein firstly describe.

The insets of the Fig. 3Ai and Bi illustrate the currents evoked by a depolarizing pulse to a moderate potential (0 mV in the case of the N1E-115 cell and to −30 mV for the CA1 neurone); in either case

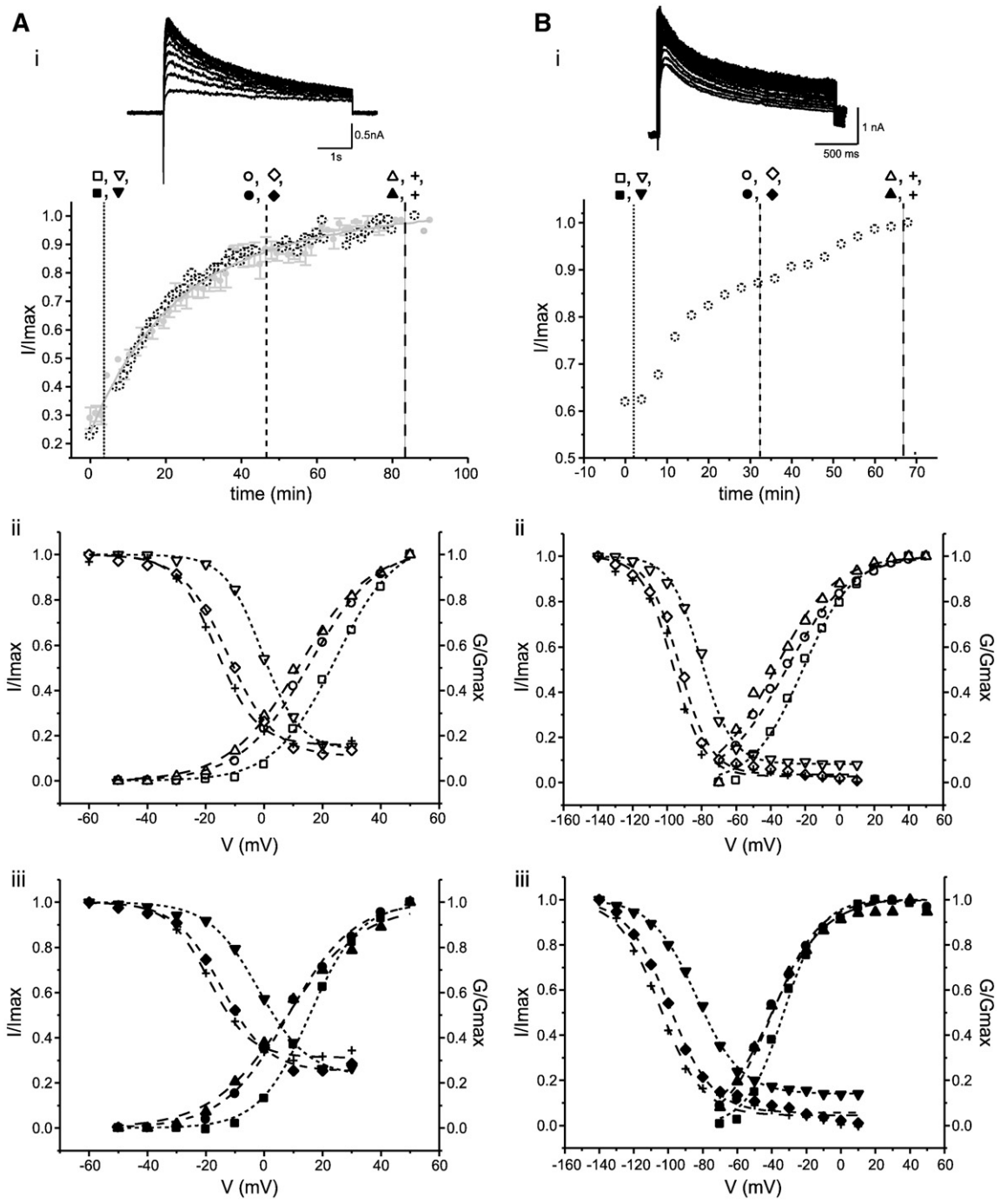

Fig. 3. Current run-up and shifts in voltage-dependence as a function of time, for N1E-115 cells (A) and for CA1 neurones (B). (Ai, Bi) Currents evoked by a depolarizing command step to 0 mV, in a (Ai) differentiated N1E-115 cell (current traces in the insert—every 10 min) and in a (Bi) a CA1 neurone (current traces in the inset—every 5 min) as a function of time after whole-cell configuration. Normalized peak current amplitude versus time after stabilization of whole-cell configuration (current run-up) for the data in the insets. Open circles with dotted line refer to the recording of the insets; for N1E-115 cells, grey points represent mean ± S.E.M. of five cells. Vertical dashed lines delimit two distinct stages of evolution of current amplitude observed in the N1E-115 cell and on CA1 neurones; symbols on top of vertical lines refer to the acquisition-timing of voltage protocols for the activation and inactivation profiles (see below). (Aii, Aiii) Steady-state inactivation and activation curves for the fast (open symbols) and slow components (closed symbols), respectively, at the three different intervals from the experiment represented in 'Ai' (N1E-115 cell). (Bii, Biii) Steady-state inactivation and activation curves for the fast (open symbols) and slow components (closed symbols), respectively, at the three different intervals from the experiment represented in 'Bi' (CA1 neurones).

pulses were applied at regular intervals in a time span of 70–90 min. An increase in current amplitude with time is clear in those current recordings; in all cases, one observed a substantial current run-up for at least 45 min after whole-cell configuration. The plot in Fig. 3Ai depicts the increase in peak current amplitude as a function of time for the N1E-115 cell illustrated in the respective inset; current run-up evolved bi-exponentially (not shown), and the same applied to CA1 neurones (Fig. 3Bi).

Such run-up could reflect time-dependent shifts in the voltage-dependence of steady-state inactivation and activation that could affect our measurements. Therefore, the voltage-dependence of steady-state inactivation and activation was studied at three different time-intervals, corresponding to the limits of the two phases of current run-up (vertical lines in Fig. 3Ai and Bi). Current amplitude values for *I*fast and *I*slow were converted to conductance, G (Eq. (2)), normalized to the maximal value, *G*/*G*max, and plotted versus step command potential, *V*, to define the voltage-dependence of activation; data points were fitted with Eq. (3). For steady-state inactivation, current values, *I*, were normalized to maximal value, *I*/*I*max, and plotted against pre-pulse potentials, *V*; data points were fitted with Eq. (4).

For the experiments with N1E-115, cells the steady-state inactivation and activation curves for *I*fast and *I*slow from the experiment represented in Fig. 3Ai with open circles are shown in Fig. 3Aii and Aiii, respectively. For the early period—corresponding to the higher rate of current run-up—the voltage shifts were as follows: $\Delta V_{1/2}$(*I*fast) = −8.9 mV, $\Delta V_{1/2}$(*I*slow) = −7.4 mV, for activation; $\Delta V_{1/2}$(*I*fast) = −11.3 mV, $\Delta V_{1/2}$(*I*slow) = −12.7 mV, for steady-state inactivation. On the other hand, during the later time period, when the rate of current run-up was slower, smaller voltage shifts were observed: $\Delta V_{1/2}$(*I*fast) = −3.5 mV, $\Delta V_{1/2}$(*I*slow) = −0.7 mV, for activation; $\Delta V_{1/2}$(*I*fast) = −4.3 mV, $\Delta V_{1/2}$(*I*slow) = −4.4 mV, for steady-state inactivation. Pooled voltage shift values (in mV/min), from 5 experiments, are summarized in Table 1. These results show that in whole-cell configuration, currents from differentiated N1E-115 cells display artefactual hyperpolarizing shifts on the steady-state inactivation and activation of *I*fast and *I*slow as a function of time. The noticeable decrease in the voltage shifts observed during the later phase of the recording relates to the later phase of the softer current run-up rate observed at 0 mV (Fig. 3Ai).

From the plots in Fig. 3Bii and Biii, it is apparent that shifts of the same nature were also observed in CA1 neurones. During the first time period (higher rate of current run-up) the voltage shifts were as follows: $\Delta V_{1/2}$(*I*fast) = −9.6 mV, $\Delta V_{1/2}$(*I*slow) = −6.4 mV, for activation; $\Delta V_{1/2}$(*I*fast) = −12.6 mV, $\Delta V_{1/2}$(*I*slow) = −15.8 mV, for steady-state inactivation. For the second time period (slower rate of current run-up), smaller voltage shifts were observed: $\Delta V_{1/2}$(*I*fast) = −6.6 mV, $\Delta V_{1/2}$(*I*slow) = −0.4 mV, for activation; $\Delta V_{1/2}$(*I*fast) = −3.7 mV, $\Delta V_{1/2}$(*I*slow) = −5.3 mV, for steady-state inactivation. Pooled data from similar recordings are summarized in Table 1.

These data revealed that the existence of such experimental artefacts that affect voltage-dependence as a function of time in whole-cell configuration may lead to misleading conclusions in the study of drug-induced voltage shifts. The mentioned voltage shifts become much smaller after 30–45 min recording. Consequently, in the experiments concerning the study of the effect of galantamine on the steady-state inactivation and activation—as described below—we accounted for the time-dependent voltage shift by waiting enough time for the start of each experiment. Measurements and drug application were carried out at the stage of minimal shifts (Fig. 3Ai and Bi, interval between 2nd and 3rd vertical dashed lines), i.e. after about 30–45 min post whole-cell configuration.

Table 1

		Early recording period		Later recording period		*n*
		$V_{1/2}$ (mV/min)	V_s (mV/e/min)	$V_{1/2}$ (mV/min)	V_s (mV/e/min)	
Activation						
N1E-115	*I*fast	−0.26 ± 0.05	0.07 ± 0.02	−0.16 ± 0.02	0.03 ± 0.01	5
	*I*slow	−0.25 ± 0.06	0.10 ± 0.03	−0.16 ± 0.03	0.08 ± 0.01	5
CA1	*I*fast	−0.47 ± 0.07	0.08 ± 0.03	−0.14 ± 0.03	0.05 ± 0.02	4
	*I*slow	−0.31 ± 0.04	0.09 ± 0.02	−0.09 ± 0.02	0.07 ± 0.03	4
Inactivation						
N1E-115	*I*fast	−0.37 ± 0.04	−0.03 ± 0.01	−0.18 ± 0.04	−0.01 ± 0.01	5
	*I*slow	−0.43 ± 0.08	−0.03 ± 0.02	−0.25 ± 0.03	0.00 ± 0.04	5
CA1	*I*fast	−0.62 ± 0.08	−0.04 ± 0.02	−0.15 ± 0.02	−0.02 ± 0.02	4
	*I*slow	−0.66 ± 0.11	−0.05 ± 0.03	−0.17 ± 0.04	−0.03 ± 0.04	4

3.4. Lack of effect of galantamine on the voltage-dependence of steady-state inactivation and activation of Islow and Ifast

To study the effect of galantamine on the voltage-dependence of steady-state inactivation and activation of *I*slow and *I*fast, current run-up at 0 mV was monitored prior to the experiment (see above). Given the dual dose–response relationship, in N1E-115 cells (Fig. 2C; square symbols), the effect of galantamine on the voltage-dependence of steady-state inactivation and activation of *I*fast and *I*slow was studied at two concentrations—100 pM and 10 μM—representative of the different phases of the dose–response relationship; 10 μM was applied in experiments with CA1 neurones.

Fig. 4A illustrates a typical effect of 100 pM (Fig. 4Ai and ii) and 10 μM galantamine (Fig. 4Aiii and iv) on the steady-state inactivation and activation curves of *I*fast and *I*slow in two differentiated N1E-115 cells; data were obtained with the corresponding protocols (insets of Fig. 1Aii–iii). The effects of 100 pM and 10 μM on the steady-state inactivation and activation parameters are summarized in pooled values in Table 2. The shifts in $V_{1/2}$ determined by galantamine in experiments carried out under the criteria described above (i.e. at the stage of minimal voltage shifts) were not statistically significant (Wilcoxon signed-rank test).

In CA1 neurones similar results were obtained, i.e. the application of 10 μM galantamine did not affect the steady-state inactivation and activation curves of *I*fast and *I*slow. Fig. 4Bi–ii show the steady-state inactivation and activation curves of *I*fast and *I*slow before and under 10 μM galantamine, in a CA1 neurone; data were obtained with the corresponding protocols (insets of Fig. 2Bii–iii). The effects of 10 μM on the steady-state inactivation and activation parameters are also summarized in polled values in Table 2.

Altogether, these results show that galantamine inhibits *I*slow in differentiated N1E-115 cells and in dissociated CA1 neurones by a process that does not involve changes in the voltage-dependence of steady—state inactivation and activation. This absence of galantamine effect on the current voltage-dependence contradicts what was previously reported (Pan et al., 2003b; Zhang et al., 2004a).

4. Discussion

The purpose of this study was to further characterize the effect of galantamine on voltage-activated K^+ currents, using two neural cell models with different origins, one from the sympathetic nervous system and the other from the brain. Our results demonstrate that galantamine (doses ranging from picomolar to micromolar) inhibits selectively a slowly inactivating K^+ current (here termed *I*slow) in a dual dose-dependent manner. These results were observed in both differentiated N1E-115 cells and in dissociated CA1 hippocampal pyramidal neurones, indicating that the reported effect of galantamine on K^+ currents may be a widespread mechanism. We also show that galantamine does not shift the activation and inactivation curves of *I*slow, as suggested previously (Pan et al., 2003b; Zhang et al., 2004a). The present findings are in part consistent with such previous studies showing that galantamine at concentrations ≥100 nM inhibits a delayed rectifier K^+ current ($I_{K(DR)}$) in dissociated rat CA1 pyramidal neurones (1–100 μM galantamine; Pan et al., 2003b) and cloned Kv2.1 channel current (0.1–100 μM; Zhang et al., 2004a). In addition, we present the first evidence that galantamine-induced inhibition of K^+ currents is also observed at concentrations under 100 nM and this effect is dose-dependent.

The dual dose response could be the result of two different K^+ currents being affected by galantamine, each one at a different concentration ranges. Indeed there are evidences that AHP, in particular

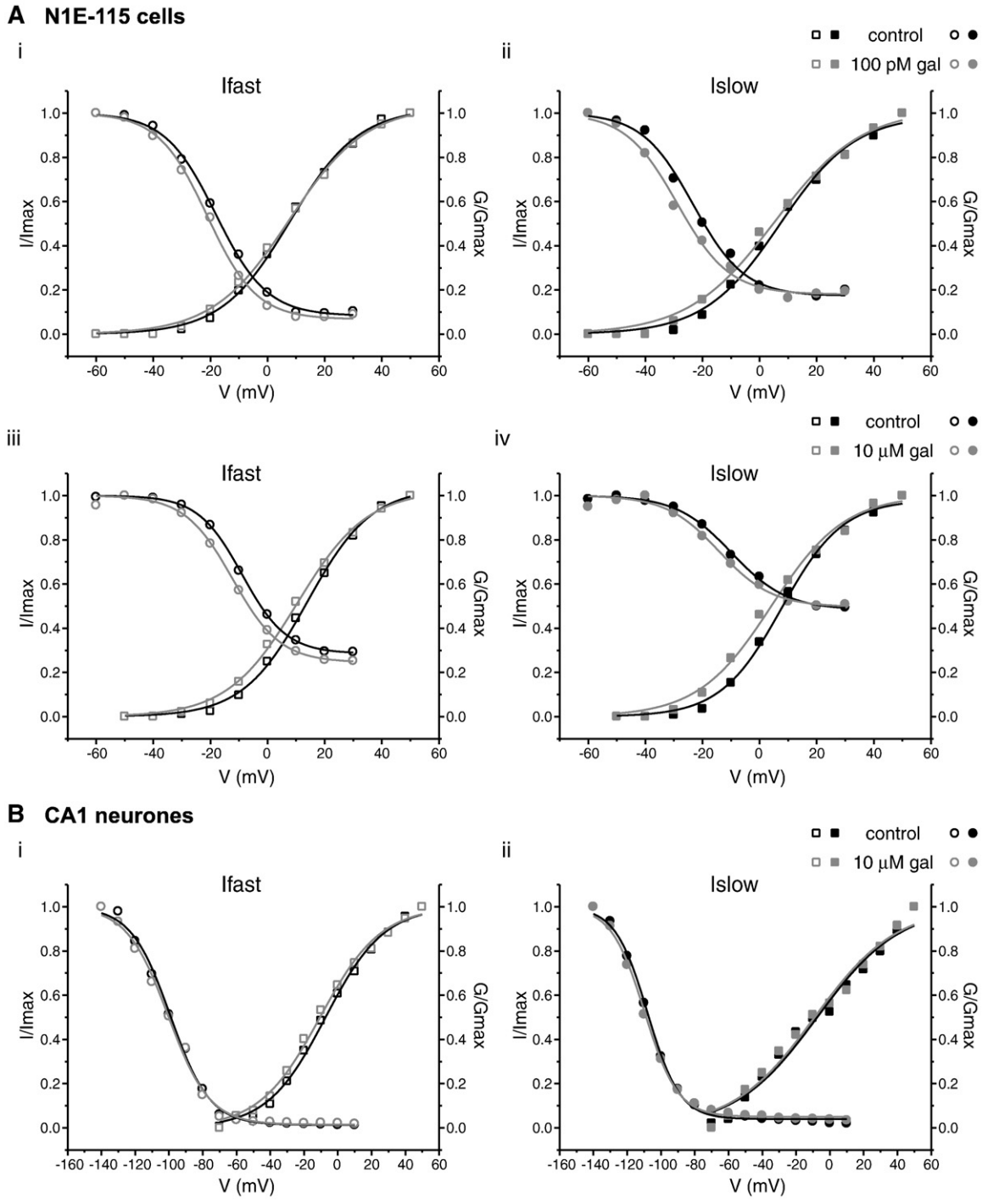

Fig. 4. Effect of galantamine (100 pM and 10 μM) on the voltage-dependence of steady-state inactivation and activation. (Ai, Aii) Typical examples of steady-state inactivation and activation curves for the fast (open symbols) and slow components (filled symbols), respectively, before (black symbols) and under 100 pM galantamine (grey symbols) in a differentiated N1E-115 cell. (Aiii, Aiv) Effect of 10 μM galantamine on the fast and slow components, respectively, in a differentiated N1E-115 cell. (Bi, Bii) Same as above (result of the application of 10 μM galantamine) in a CA1 neurone. Results relate to typical individual experiments; pooled data is presented in Table 2. For the voltage-dependence of activation, the amplitudes of the fast and slow components were converted to conductance (Eq. (2)) and normalized to maximal conductance; normalized data points were fit with Eq. (3). For steady-state inactivation, the amplitudes of the fast and slow components were normalized to maximal current and fit with Eq. (4). For the experiment with 100 pM galantamine applied to a N1E-115 cell (Ai, Aii), the fitting parameters concerning both current components were as follows: for activation curves—*I*fast (control, $V_{1/2}=8.1$ mV, $V_s=12.2$ mV/e; galantamine $V_{1/2}=7.8$ mV, $V_s=13.9$ mV/e) and *I*slow (control, $V_{1/2}=6.5$ mV, $V_s=15.2$ mV/e; galantamine $V_{1/2}=4.6$ mV, $V_s=19.0$ mV/e); for steady-state inactivation curves—*I*fast (control, $V_{1/2}=-19.2$ mV, $V_s=-8.4$ mV/e; galantamine $V_{1/2}=-21.8$ mV, $V_s=-7.9$ mV/e) and *I*slow (control, $V_{1/2}=-24.4$ mV, $V_s=-8.9$ mV/e; galantamine $V_{1/2}=-30.7$ mV, $V_s=-9.6$ mV/e). For the experiment with 10 μM galantamine applied to a N1E-115 cell (aiii, aiv), the fitting parameters were: for activation curves—*I*fast (control, $V_{1/2}=13.8$ mV, $V_s=11.5$ mV/e; galantamine $V_{1/2}=10.3$ mV, $V_s=12.8$ mV/e) and *I*slow (control, $V_{1/2}=7.4$ mV, $V_s=11.5$ mV/e; galantamine $V_{1/2}=3.7$ mV, $V_s=14.5$ mV/e); for steady-state inactivation curves—*I*fast (control, $V_{1/2}=-10.8$ mV, $V_s=-6.3$ mV/e; galantamine $V_{1/2}=-14.1$ mV, $V_s=-6.4$ mV/e) and *I*slow (control, $V_{1/2}=-9.8$ mV, $V_s=-9.6$ mV/e; galantamine $V_{1/2}=-13.5$ mV, $V_s=-8.5$ mV/e). For the experiment with 10 μM galantamine applied to a CA1 neurone (Bi, Bii), the fitting parameters were: for activation curves—*I*fast (control, $V_{1/2}=-7.2$, $V_s=17.3$ mV/e; galantamine $V_{1/2}=10.5$ mV, $V_s=17.8$ mV/e) and *I*slow (control, $V_{1/2}=-7.6$ mV, $V_s=24.3$ mV/e; galantamine $V_{1/2}=-9.1$ mV, $V_s=24.2$ mV/e); for steady-state inactivation curves—*I*fast (control, $V_{1/2}=-99.2$ mV, $V_s=-11.6$ mV/e; galantamine $V_{1/2}=-100.5$ mV, $V_s=-11.9$ mV/e) and *I*slow (control, $V_{1/2}=-107.9$ mV, $V_s=-9.7$ mV/e; galantamine $V_{1/2}=-109.6$ mV, $V_s=-9.8$ mV/e). All experiments started after 30–45 min recording to account for the voltage shifts described above (Fig. 3, Table 1); voltage protocols prior to galantamine application were just applied after a negligible current run-up being observed (described in Fig. 3Ai and Bi).

Table 2

		Control		Galantamine		
		$V_{1/2}$ (mV)	V_s (mV/e)	$V_{1/2}$ (mV)	V_s (mV/e)	n
Activation						
N1E-115	100 pM					
	*I*fast	13.0 ± 2.5	12.3 ± 0.4	9.6 ± 3.3	13.7 ± 0.6	5
	*I*slow	10.3 ± 2.6	13.8 ± 0.7	8.4 ± 3.6	20.4 ± 0.7	5
	10 μM					
	*I*fast	14.1 ± 1.1	12.6 ± 1.0	9.2 ± 1.7	14.0 ± 1.3	5
	*I*slow	8.9 ± 1.4	12.2 ± 0.5	4.1 ± 2.4	16.0 ± 0.9	5
CA1	10 μM					
	*I*fast	−16.6 ± 2.9	14.1 ± 1.0	−20.7 ± 3.0	14.6 ± 0.9	3
	*I*slow	−18.6 ± 1.7	18.5 ± 0.9	−20.4 ± 2.1	18.2 ± 0.8	3
Inactivation						
N1E-115	100 pM					
	*I*fast	−16.5 ± 1.4	−8.1 ± 0.6	−20.5 ± 1.2	−7.9 ± 0.6	5
	*I*slow	−20.8 ± 2.5	−8.4 ± 0.5	−26.6 ± 2.4	−8.7 ± 0.6	5
	10 μM					
	*I*fast	−10.0 ± 0.7	−7.9 ± 0.4	−13.5 ± 0.6	−8.2 ± 0.5	5
	*I*slow	−15.2 ± 2.2	−8.0 ± 0.8	−19.9 ± 2.1	−8.9 ± 1.5	5
CA1	10 μM					
	*I*fast	−96.8 ± 0.9	−9.4 ± 0.8	−98.7 ± 2.6	−9.9 ± 0.9	3
	*I*slow	−99.6 ± 2.9	−9.9 ± 1.1	−99.2 ± 3.0	−10.2 ± 1.2	3

its slow component, is inhibited by galantamine in CA1 pyramidal neurons (Oh et al., 2006). However, it is unlikely that the slow AHP current was evoked with the voltage protocols used here considering (a) the voltage-dependence of *I*slow and (b) the time course of the rising phase of the slow AHP current. Moreover, in the present study, the time constant values of the exponential decay of the galantamine-sensitive currents are not different for both galantamine concentrations (100 pM and 10 μM). Also, with both representative concentrations, galantamine is inhibiting *I*slow in a similar way, i.e., not changing the voltage profiles. Altogether, there are strong suggestions that it is the same current being affected in the two galantamine concentration ranges of the dual dose–response relationship.

It has been reported that acetylcholine can control K^+ currents through mechanisms mediated by nicotinic receptors (Hamon et al., 1997). Therefore, the observed galantamine-induced K^+ current reduction could eventually be a consequence of the inhibition of AChE, as it would lead to the increase of acetylcholine levels. However, that seems not to be the case in the present study, as recordings were performed under continuous superfusing solution (not containing acetylcholine). For galantamine concentrations ranging from 1 pM to 100 nM, the hypothesis of AChE inhibition as the cause for galantamine-induced current reduction is even less likely; i.e. such concentrations are not within the IC_{50} range (0.4–4 μM) of brain cholinesterase inhibition by galantamine (Bickel et al., 1991; Sweeney et al., 1989; Bores et al., 1996).

The relevance of the inhibition of K^+ currents by AChE inhibitors to Alzheimer's disease therapy is still not clear. It has been suggested that tacrine (one of the others AChE inhibitors currently used in Alzheimer's disease therapy) could enhance neurotransmitter release into the synaptic cleft, by inhibiting $I_{K(DR)}$ and increasing the duration of action potentials, as observed in Drosophila larval muscles (Kraliz and Singh, 1997). Several reports have suggested a link between Alzheimer's disease and K^+ channels. For example, in fibroblasts obtained from patients with Alzheimer's disease, a K^+ channel dysfunction was discovered (Etcheberrigaray et al., 1993); this could be mimicked in normal fibroblasts by the addition of β-amyloid peptide (Aβ) (Etcheberrigaray et al., 1994). In cortical neurones and septal cholinergic cells, exposure to Aβ enhanced $I_{K(DR)}$ (Yu et al., 1998; Colom et al., 1998, respectively); Aβ-induced neuronal death could be attenuated by the addition of tetraethylammonium (Yu et al., 1998). Furthermore, overexpression of presenilin-1, presenilin-2 and amyloid precursor protein—the respective genes are associated with hereditary Alzheimer's disease—increased $I_{K(DR)}$ in rat hippocampal pyramidal neurones, which might be related to neuronal apoptosis (Zhang et al., 2004c). Overall, these studies suggest that the inhibition of delayed rectifier-like currents by AChE inhibitors, and therefore by galantamine, may lead to the suppression of apoptosis and to a substantial increase in cell survival.

A relevant issue deals with the concentration of galantamine used in in vitro experiments and the levels reached in the brain of patients and animals. Although there is some uncertainty about the actual brain concentrations of galantamine in Alzheimer's disease patients (Jann et al., 2002), it is estimated that for patients treated with doses of 16–24 mg/day, brain galantamine concentration ranges from 0.5 to 1.2 μM (values extrapolated from Marco-Contelles et al., 2006). In the case of mice, galantamine doses between 1.5 and 5 mg/kg achieve brain levels in the range of 0.2–1 μM (Marco-Contelles et al., 2006). According to the previous reports by Pan et al. (2003b) and Zhang et al. (2004a) concerning galantamine effect on voltage-activated K^+ currents, galantamine seems to be effective only at micromolar concentrations (Pan et al., 2003b; Zhang et al., 2004a), i.e. at concentrations higher than those reached in clinical conditions. Therefore, our results are particularly relevant in the context of clinical applications of galantamine, since they show for the first time that galantamine-induced inhibition of K^+ currents, at concentrations under 100 nM, might contribute to the effectiveness of galantamine in the treatment of Alzheimer's disease.

In the present study, we observed that recordings from both differentiated N1E-115 cells and CA1 neurones display artefactual hyperpolarizing shifts on the steady-state inactivation and activation curves of *I*fast and *I*slow (smaller shifts for *I*fast). These shifts in voltage-dependence evolved in time with two distinct rates: a faster rate, which lasted about 30–45 min after whole-cell configuration; a slower rate, which continued throughout the recording period. Similar shifts were observed previously with Na^+ currents in the whole-cell configuration (Sakmann and Neher, 1995); peak current and steady-state activation curves showed a negative shift after 30 min of whole-cell recording. Additionally, signs of a hyperpolarizing voltage shift were also found in the analysis of Ca^{2+} currents (Fenwick et al., 1982). It has been suggested that these shifts in the voltage-dependence result from the existence of junction potentials between different solutions, namely between pipette solution and citosol (Sakmann and Neher, 1995), although, shifts along the voltage axis may also result from other effects. For instance, during the course of whole-cell recording, membrane proteins may undergo phosphorylation/dephosphorylation as a result of inevitable changes in citosol composition (Sakmann and Neher, 1995); e.g. large hyperpolarizing shifts in voltage-dependent activation of Kv2.1-based neuronal IK were observed under conditions leading to Kv2.1 dephosphorylation (e.g. Misonou et al., 2005, 2004; Murakoshi et al., 1997).

By considering these artefactual voltage shifts into our experimental procedures, we allowed our results to demonstrate that galantamine-induced current inhibition is not due to a shift in the voltage-dependence of steady-state inactivation and activation. The small hyperpolarizing shifts that were observed before and under galantamine, when confronted with the artefactual voltage shifts seen during the second time period of current run-up, became meaningless. These results are in disagreement with the studies of Pan et al. (2003b) and Zhang et al. (2004a), that report that galantamine shifts the activation and inactivation curves of $I_{K(DR)}$ to negative potentials. According to such studies, the shift on the inactivation was more pronounced (Pan et al., 2003b; Zhang et al., 2004a) (interestingly, the artefactual shifts reported here, are also more pronounced for the inactivation profiles) . Also, a hyperpolarizing shift on the activation curve indicates activation at lower potentials that normally results in an increase in current amplitude. Therefore, the K^+ current reduction observed in both studies conflicts with the hyperpolarizing shift on the activation curve. Our results also contrast with what has been noted for other AChE inhibitors whose inhibitory effects on K^+ currents have been

related to similar voltage shifts: donepezil (Zhong et al., 2002); rivastigmine (Pan et al., 2003b); huperzine A (Li and Hu, 2002).

The present report provides the first evidence of a dual dose–response relationship for the inhibition of a slowly inactivating K^+ current by galantamine, in differentiated N1E-115 cells and in CA1 neurones. It also describes the existence of an important experimental artefact that affects voltage-dependence as a function of time in whole-cell configuration; monitoring such artefacts is of paramount importance as they may lead to misleading conclusions in the study of drug-induced voltage shifts. Finally, we demonstrate that galantamine-induced current inhibition does not occur via a shift in the voltage-dependence of steady-state inactivation and activation, as opposed to what was previously suggested.

Acknowledgments

PAL was supported by the Fundação Ciência e Tecnologia FCT (SFRH/BPD/18969/2004-09-07 and Ciência 2007). We wish to thank Frederico M. Alves for experimental assistance and Ana I. Santos and Isabel R. da Silva for cell-culture assistance.

References

Barnes, C.A., Meltzer, J., Houston, F., Orr, G., McGann, K., Wenk, G.L., 2000. Chronic treatment of old rats with donepezil or galantamine: effects on memory, hippocampal plasticity and nicotinic receptors. Neuroscience 99, 17–23.

Bartus, R.T., Dean III, R.L., Beer, B., Lippa, A.S., 1982. The cholinergic hypothesis of geriatric memory dysfunction. Science 217, 408–414.

Bickel, U., Thomsen, T., Fischer, J.P., Weber, W., Kewitz, H., 1991. Galanthamine: pharmacokinetics, tissue distribution and cholinesterase inhibition in brain of mice. Neuropharmacology 30, 447–454.

Bores, G.M., Huger, F.P., Petko, W., Mutlib, A.E., Camacho, F., Rush, D.K., Selk, D.E., Wolf, V., Kosley Jr., R.W., Davis, L., Vargas, H.M., 1996. Pharmacological evaluation of novel Alzheimer's disease therapeutics: acetylcholinesterase inhibitors related to galanthamine. J. Pharmacol. Exp. Ther. 277, 728–738.

Caricati-Neto, A., D'Angelo, L.C., Reuter, H., Hyppolito Jurkiewicz, N., Garcia, A.G., Jurkiewicz, A., 2004. Enhancement of purinergic neurotransmission by galantamine and other acetylcholinesterase inhibitors in the rat vas deferens. Eur. J. Pharmacol. 503, 191–201.

Chen, X., Yuan, L.L., Zhao, C., Birnbaum, S.G., Frick, A., Jung, W.E., Schwarz, T.L., Sweatt, J. D., Johnston, D., 2006. Deletion of Kv4.2 gene eliminates dendritic A-type K^+ current and enhances induction of long-term potentiation in hippocampal CA1 pyramidal neurons. J. Neurosci. 26, 12143–12151.

Colom, L.V., Diaz, M.E., Beers, D.R., Neely, A., Xie, W.J., Appel, S.H., 1998. Role of potassium channels in amyloid-induced cell death. J. Neurochem. 70, 1925–1934.

Costa, P.F., Santos, A.I., Ribeiro, M.A., 1994. Potassium currents in acutely isolated maturing rat hippocampal CA1 neurones. Brain Res. Dev. Brain Res. 83, 216–223.

Etcheberrigaray, R., Ito, E., Oka, K., Tofel-Grehl, B., Gibson, G.E., Alkon, D.L., 1993. Potassium channel dysfunction in fibroblasts identifies patients with Alzheimer disease. Proc. Natl. Acad. Sci. U. S. A. 90, 8209–8213.

Etcheberrigaray, R., Ito, E., Kim, C.S., Alkon, D.L., 1994. Soluble beta-amyloid induction of Alzheimer's phenotype for human fibroblast K^+ channels. Science 264, 276–279.

Farlow, M.R., 2003. Clinical pharmacokinetics of galantamine. Clin. Pharmacokinet. 42, 1383–1392.

Fenwick, E.M., Marty, A., Neher, E., 1982. Sodium and calcium channels in bovine chromaffin cells. J. Physiol. 331, 599–635.

Francis, P.T., Palmer, A.M., Snape, M., Wilcock, G.K., 1999. The cholinergic hypothesis of Alzheimer's disease: a review of progress. J. Neurol. Neurosurg. Psychiatry 66, 137–147.

Hamon, B., Glowinski, J., Giaume, C., 1997. Nicotine inhibits slowly inactivating K^+ currents in rat cultured striatal neurons. Pflugers Arch. 434, 642–645.

Inan, S.Y., Aksu, F., Baysal, F., 2000. The effects of some K(+) channel blockers on scopolamine- or electroconvulsive shock-induced amnesia in mice. Eur. J. Pharmacol. 407, 159–164.

Jann, M.W., Shirley, K.L., Small, G.W., 2002. Clinical pharmacokinetics and pharmacodynamics of cholinesterase inhibitors. Clin. Pharmacokinet. 41, 719–739.

Kraliz, D., Singh, S., 1997. Selective blockade of the delayed rectifier potassium current by tacrine in Drosophila. J. Neurobiol. 32, 1–10.

Li, Y., Hu, G.Y., 2002. Huperzine A inhibits the sustained potassium current in rat dissociated hippocampal neurons. Neurosci. Lett. 329, 153–156.

Lilienfeld, S., 2002. Galantamine—a novel cholinergic drug with a unique dual mode of action for the treatment of patients with Alzheimer's disease. CNS Drug Rev. 8, 159–176.

Lima, P.A., Vicente, M.I., Alves, F.M., Dionisio, J.C., Costa, P.F., 2008. Insulin increases excitability via a dose-dependent dual inhibition of voltage-activated K^+ currents in differentiated N1E-115 neuroblastoma cells. Eur. J. NeuroSci. 27, 2019–2032.

Lisman, J., 2003. Long-term potentiation: outstanding questions and attempted synthesis. Philos. Trans. R. Soc. Lond. B Biol. Sci. 358, 829–842.

Maelicke, A., Coban, T., Storch, A., Schrattenholz, A., Pereira, E.F., Albuquerque, E.X., 1997. Allosteric modulation of Torpedo nicotinic acetylcholine receptor ion channel activity by noncompetitive agonists. J. Recept. Signal Transduct. Res. 17, 11–28.

Marco-Contelles, J., do Carmo Carreiras, M., Rodriguez, C., Villarroya, M., Garcia, A.G., 2006. Synthesis and pharmacology of galantamine. Chem. Rev. 106, 116–133.

Misonou, H., Mohapatra, D.P., Park, E.W., Leung, V., Zhen, D., Misonou, K., Anderson, A.E., Trimmer, J.S., 2004. Regulation of ion channel localization and phosphorylation by neuronal activity. Nat. Neurosci. 7, 711–718.

Misonou, H., Mohapatra, D.P., Menegola, M., Trimmer, J.S., 2005. Calcium- and metabolic state-dependent modulation of the voltage-dependent Kv2.1 channel regulates neuronal excitability in response to ischemia. J. Neurosci. 25, 11184–11193.

Moriguchi, S., Marszalec, W., Zhao, X., Yeh, J.Z., Narahashi, T., 2004. Mechanism of action of galantamine on N-methyl-D-aspartate receptors in rat cortical neurons. J. Pharmacol. Exp. Ther. 310, 933–942.

Murakoshi, H., Shi, G., Scannevin, R.H., Trimmer, J.S., 1997. Phosphorylation of the Kv2.1 K^+ channel alters voltage-dependent activation. Mol. Pharmacol. 52, 821–828.

Oh, M.M., Wu, W.W., Power, J.M., Disterhoft, J.F., 2006. Galantamine increases excitability of CA1 hippocampal pyramidal neurons. Neuroscience 137, 113–123.

Pan, Y., Xu, X., Wang, X., 2003a. Rivastigmine blocks voltage-activated K^+ currents in dissociated rat hippocampal neurons. Br. J. Pharmacol. 140, 907–912.

Pan, Y.P., Xu, X.H., Wang, X.L., 2003b. Galantamine blocks delayed rectifier, but not transient outward potassium current in rat dissociated hippocampal pyramidal neurons. Neurosci. Lett. 336, 37–40.

Pleumsamran, A., Wolak, M.L., Kim, D., 1998. Inhibition of ATP-induced increase in muscarinic K^+ current by trypsin, alkaline pH, and anions. Am. J. Physiol. 275, H751–H759.

Ramakers, G.M., Storm, J.F., 2002. A postsynaptic transient K(+) current modulated by arachidonic acid regulates synaptic integration and threshold for LTP induction in hippocampal pyramidal cells. Proc. Natl. Acad. Sci. U. S. A. 99, 10144–10149.

Raskind, M.A., Peskind, E.R., Wessel, T., Yuan, W., 2000. Galantamine in AD: a 6-month randomized, placebo-controlled trial with a 6-month extension. The Galantamine USA-1 Study Group. Neurology 54, 2261–2268.

Sakmann, B., Neher, E., 1995. Single-channel Recording, 2nd ed. Plenum, New York.

Samochocki, M., Zerlin, M., Jostock, R., Groot Kormelink, P.J., Luyten, W.H., Albuquerque, E.X., Maelicke, A., 2000. Galantamine is an allosterically potentiating ligand of the human alpha4/beta2 nAChR. Acta Neurol. Scand. Suppl. 176, 68–73.

Santos, M.D., Alkondon, M., Pereira, E.F., Aracava, Y., Eisenberg, H.M., Maelicke, A., Albuquerque, E.X., 2002. The nicotinic allosteric potentiating ligand galantamine facilitates synaptic transmission in the mammalian central nervous system. Mol. Pharmacol. 61, 1222–1234.

Schilstrom, B., Ivanov, V.B., Wiker, C., Svensson, T.H., 2007. Galantamine enhances dopaminergic neurotransmission in vivo via allosteric potentiation of nicotinic acetylcholine receptors. Neuropsychopharmacology 32, 43–53.

Schrattenholz, A., Pereira, E.F., Roth, U., Weber, K.H., Albuquerque, E.X., Maelicke, A., 1996. Agonist responses of neuronal nicotinic acetylcholine receptors are potentiated by a novel class of allosterically acting ligands. Mol. Pharmacol. 49, 1–6.

Sweeney, J.E., Puttfarcken, P.S., Coyle, J.T., 1989. Galanthamine, an acetylcholinesterase inhibitor: a time course of the effects on performance and neurochemical parameters in mice. Pharmacol. Biochem. Behav. 34, 129–137.

Thomsen, T., Kewitz, H., 1990. Selective inhibition of human acetylcholinesterase by galanthamine in vitro and in vivo. Life Sci. 46, 1553–1558.

Thomsen, T., Kaden, B., Fischer, J.P., Bickel, U., Barz, H., Gusztony, G., Cervos-Navarro, J., Kewitz, H., 1991. Inhibition of acetylcholinesterase activity in human brain tissue and erythrocytes by galanthamine, physostigmine and tacrine. Eur. J. Clin. Chem. Clin. Biochem. 29, 487–492.

Wilcock, G.K., Lilienfeld, S., Gaens, E., 2000. Efficacy and safety of galantamine in patients with mild to moderate Alzheimer's disease: multicentre randomised controlled trial. Galantamine International-1 Study Group. BMJ 321, 1445–1449.

Yu, B., Hu, G.Y., 2005. Donepezil blocks voltage-gated ion channels in rat dissociated hippocampal neurons. Eur. J. Pharmacol. 508, 15–21.

Yu, S.P., Farhangrazi, Z.S., Ying, H.S., Yeh, C.H., Choi, D.W., 1998. Enhancement of outward potassium current may participate in beta-amyloid peptide-induced cortical neuronal death. Neurobiol. Dis. 5, 81–88.

Zhang, H.X., Zhang, W., Jin, H.W., Wang, X.L., 2004a. Galantamine blocks cloned Kv2.1, but not Kv1.5 potassium channels. Brain Res. Mol. Brain Res. 131, 136–140.

Zhang, L., Zhou, F.M., Dani, J.A., 2004b. Cholinergic drugs for Alzheimer's disease enhance in vitro dopamine release. Mol. Pharmacol. 66, 538–544.

Zhang, W., Jin, H.W., Wang, X.L., 2004c. Effects of presenilins and beta-amyloid precursor protein on delayed rectifier potassium channels in cultured rat hippocampal neurons. Acta Pharmacol. Sin. 25, 181–185.

Zhong, C.B., Zhang, W., Wang, X.L., 2002. Effects of donepezil on the delayed rectifier-like potassium current in pyramidal neurons of rat hippocampus and neocortex. Yao Xue Xue Bao 37, 415–418.